Neurobiology of Aging 96 (2020) 246–254

Contents lists available at ScienceDirect

Neurobiology of Aging

journal homepage: www.elsevier.com/locate/neuaging

Age-related differences in myeloarchitecture measured at 7 T

Andrew J. Carradus[a], Olivier Mougin[a], Benjamin A.E. Hunt[a], Prejaas K. Tewarie[a], Nicolas Geades[b], Peter G. Morris[a], Matthew J. Brookes[a], Penny A. Gowland[a], Christopher R. Madan[a,c,*]

[a] Sir Peter Mansfield Imaging Centre, School of Physics and Astronomy, University of Nottingham, Nottingham, UK
[b] Philips Clinical Science, Philips Healthcare, Eindhoven, the Netherlands
[c] School of Psychology, University of Nottingham, Nottingham, UK

ARTICLE INFO

Article history:
Received 10 February 2020
Received in revised form 6 August 2020
Accepted 10 August 2020
Available online 22 August 2020

Keywords:
Aging
Brain structure
Myelin
MT
7 tesla
Gray matter

ABSTRACT

We have used the magnetisation transfer (MT) MRI measure as a primary measure of myelination in both the gray matter (GM) of the 78 cortical automated anatomical labeling (AAL) regions of the brain, and the underlying white matter in each region, in a cohort of healthy adults (aged 19–62 year old). The results revealed a significant quadratic trend in myelination with age, with average global myelination peaking at 42.9 year old in gray matter, and at 41.7 year old in white matter. We also explored the possibility of using the Nuclear Overhauser Enhancement (NOE) effect, which is acquired in a similar method to MT, as an additional measure of myelination. We found that the MT and NOE signals were strongly correlated in the brain and that the NOE effects displayed similar (albeit weaker) parabolic trends with age. We also investigated differences in cortical thickness with age, and confirmed a previous result of a linear decline of 4.5 ± 1.2 μm/y.

1. Introduction

Many aspects of brain structure vary systematically as a function of age, such as cortical thickness, gyrification, subcortical volume, and white matter tract integrity (Bartzokis et al., 2012; de Mooij et al., 2018; Fjell et al., 2009; Hogstrom et al., 2013; Madan and Kensinger, 2016, 2017, 2018; Salat et al., 2004; Tamnes et al., 2010). Foundational work in the early 1900s used post-mortem histological techniques on small numbers of individuals to show age-related differences in cortical myelination (Kaes, 1907), and also provided insights into related topology (Campbell, 1905; Flechsig, 1920; Hopf, 1955; Vogt, 1906). However the data remain sparse and in vivo measures are really required to enable proper study across the life span.

Magnetic resonance imaging (MRI) provides a range of markers of myeloarchitecture and myelination in vivo (Armstrong et al., 2004; Callaghan et al., 2014; Dick et al., 2012; Glasser and Van Essen, 2011; Mangeat et al., 2015; Sanchez-Panchuelo et al., 2012) and thus provides a unique opportunity to study differences in brain myelination through life (Callaghan et al., 2014; Draganski et al., 2011; Grydeland et al., 2013). These studies used ratio of T_1 versus T_2 intensity or magnetisation transfer sequences to observe widespread age-related differences in myelination. Earlier work (Cho et al., 1997) observed a quadratic trend with in vivo human brain T_1 measurements with age, however they suggested that this differences could originate in other factors beyond myelination including differences in membrane lipid content, brain volume, and cortical iron content. Another study (Yeatman et al., 2014) measured T_1 in white matter fascicles and also found a parabolic trend with age, while in addition showing that T_1 measurements were correlated to macromolecule tissue content. Previous work (Bartzokis et al., 2012) showed differences in T_2 and diffusion measured during the life span related to brain development and brain repair, but T_2 is strongly affected by iron content and diffusion measures depend on axonal geometry.

Magnetisation transfer (MT) imaging has been used to study myelination in a number of prior studies (Armstrong et al., 2004; Callaghan et al., 2014; Zaretskaya et al., 2018), providing an advantage over T_1 based measures in that when quantified correctly, the quantitative MT signal is not affected by cortical iron content (Lorio et al., 2014). Here we sought to examine age-related differences in myelination at 7 T using both quantitative MT and the related Nuclear Overhauser Enhancement (NOE) effect and provide more specific regional estimates of these effects.

While conventional MRI observes the properties of unrestricted cellular ('free') water protons, there are other 'bound' protons that

* Corresponding author at: School of Psychology, University Park, University of Nottingham, Nottingham NG7 2RD, UK. Tel.: +44 (0)115 951 5365; fax: +44 (0)115 951 3666.
E-mail address: christopher.madan@nottingham.ac.uk (C.R. Madan).

0197-4580/$ – see front matter © 2020 Elsevier Inc. All rights reserved.
https://doi.org/10.1016/j.neurobiolaging.2020.08.009

also contribute to the MR signal. These consist of both macromolecular protons, and certain water protons which have their motion restricted through hydrogen bonding to the macromolecular surface. We can probe the presence of these macromolecules via the MT effect (Wolff and Balaban, 1989), by selectively saturating the bound protons (which resonate at a frequency which is off-resonance from free water). As the bound protons return to equilibrium they can transfer their magnetisation to free water, primarily through dipole-dipole interactions (Edzes et al., 1977), and the resulting reduction in the free water signal can be detected using conventional MRI methods.

The NOE signal is acquired in a similar way, except that the NOE signal corresponds to protons resonating specifically at −3.5 ppm with respect to water (Jones et al., 2013). Details of the physical origins of this signal are given elsewhere, but in short the NOE signal occurs when energy is exchanged between 2 spins that are very close together (~0.5 nm), and it is generally associated with aliphatic and olefinic protons (Desmond et al., 2014). NOE and MT signals seem to vary in a similar way in the healthy brain, however this is not the case in all tissues (Shah et al., 2018). MRI at 7 T provides increased sensitivity for MT and NOE effects and also higher signal-to-noise ratio (SNR) and hence spatial resolution, which will improve sensitivity in studies of aging. Technical issues related to increased specific absorption rate (SAR) and inhomogeneities in the B_1 transmit field can complicate the measurements, and MT measurements can also be affected by variations in T_1 so the method of quantification used here took account of B_1 and T_1 variations via a look up table.

In this study we aimed to investigate for the first time the variation of quantitative MT and NOE signals over the mid-life age range and to compare it to differences in cortical thickness.

2. Methods

2.1. Participants

Ethical approval was granted by the University of Nottingham Medical School Research Ethics Committee. From an initial recruitment of 77 people giving a written informed consent for a combined MEG/MRI study (Hunt et al., 2016), 58 participants (aged 19–62 year old; 27 male; 52 right-handed) successfully fulfilled complete data acquisition with satisfactory data quality on the FreeSurfer cortical ribbon segmentation. Participants completed an online screening form to assess health and lifestyle, which included the Edinburgh Handedness Inventory (Oldfield, 1971), and were excluded from the study if they had current mental illness or diagnosis of mental illness within 5 years, any history of neurological disorder, or family history of highly heritable mental illness (such as schizophrenia or Huntington's Chorea). It was not feasible to exclude people with any history of mental illness due to the high proportion of individuals who have, at some point, been diagnosed with a mental illness. This study is based on additional analyses of MRI data from a previously published dataset comparing magnetoencephalography and 7 T MRI (Hunt et al., 2016).

2.2. MRI acquisition

The MRI protocol has been described previously (Hunt et al., 2016), and is only summarised here. Participants were scanned using a Philips Achieva 7 T system with the Phase Sensitive Inversion Recovery sequence (PSIR: TI1/TI2=780 ms/1600 ms, 0.8 mm isotropic voxels 240 × 216 × 160 mm^3 field of view) (Mougin et al., 2016) to delineate the cortex. MT and NOE were quantified by acquiring z-spectra (Geades et al., 2016), which plot the water proton signal measured at progressively different off resonance saturation frequencies. A z-spectrum was acquired using a magnetization transfer prepared-turbo field echo (MT-TFE) sequence with a train of 20 off-resonance saturation pulses (Gaussian-windowed sinc pulses, bandwidth 200 Hz) applied at 17 frequency offsets in turn (0, ±1.0, −2.3, +2.5, ±3, ±3.5, ±4.0, +4.5, −4.7, ±6.7 and ±16.7, and also +167 ppm acquired for normalization). This was repeated at 3 nominal B_1 amplitudes ($B1_{rms}$= 0.38, 0.75, and 1.25 μT) to provide sensitivity to effects more prevalent at high or low saturation powers (Geades et al., 2016). The TFE 3D imaging readout (TE/TR/FA=2.7 ms/5.8 ms/8°) provided 1.5 mm isotropic image resolution across a FOV of 192 × 192 × 60 mm^3. The total acquisition time was 24 minutes total for the 3 powers. The z-spectra were motion corrected using FSL MCFLIRT (Woolrich et al., 2009) and B_0 corrected (Mougin et al., 2010). They were then fitted to a database of spectra simulated using the Bloch-McConnell equations (Geades et al., 2016). This fit resulted in a map of the estimate for the size of the bound proton pool without contamination from chemical exchange saturation transfer (CEST) or NOE effects, and a separate map of NOE effects.

2.3. Image analysis

The PSIR images were used to create a conservative gray matter (GM) mask and a white matter (WM) mask with no overlap between them, using the boundary detection tool in FreeSurfer v5.3.0 (Dale et al., 1999; Fischl, 2012). If a voxel lay on the boundary between the gray and white matter, it was excluded. PSIR images were then registered to the automated anatomical labeling (AAL) atlas (Tzourio-Mazoyer et al., 2002) using FSL, and the mean cortical thickness was calculated for each region within the AAL atlas, for each participant using FreeSurfer. Cortical thickness estimates were averaged across the whole brain and plotted against participant age. This was repeated for each AAL region separately and for data averaged across selections of AAL regions representative of each of the 4 lobes in the brain. A linear fit of cortical thickness against age was performed for all these conditions, and the p-values of the fit were calculated. False discovery rate (FDR) correction ($\alpha = 0.05$) was performed on the data from the individual AAL regions to correct for multiple comparisons. The PSIR data was also used to provide an estimate T_1 by comparing the signal from both readouts to a look-up table (Geades et al., 2016)

The MT maps were registered to the PSIR images and masked first with the conservative GM or WM mask, and then with the cortical AAL atlas or its underlying subcortical regions, to produce 78 GM-only and 78 WM-only ROIs for each participant, and a mean MT value was calculated for each region. MT was plotted against participant's age for both the whole GM, and averaged across regions of interest (ROIs), corresponding to the 4 lobes as for cortical thickness. Fourteen regions of the brain were excluded due to limited field of view or poor B_1 shimming in these areas (regions 1, 2, 24, 28, 32, 34, 35, 40, 63, 67, 71, 72, 73, 74 of the cortical AAL atlas primarily located at the base of the brain). Data were fitted with linear and quadratic functions and p-values of the fits were estimated. An F-test was performed to determine whether the quadratic fit described the data significantly better than the linear fit, by comparing the R^2 of each fit considering the additional degree of freedom gained with a quadratic model. The quadratic coefficient within any GM region where the quadratic fit was significant was mapped onto a cortical surface. To explore spatial variability across the cortex in individual participants, we also calculated the standard deviation of MT across gray and white matter ROIs, and cortical thickness across the whole cortex and across the 4 lobes separately. This was repeated for WM with the quadratic coefficient also projected onto the cortical surface to allow the GM and WM differences to be compared. Finally, the participant-averaged MT in

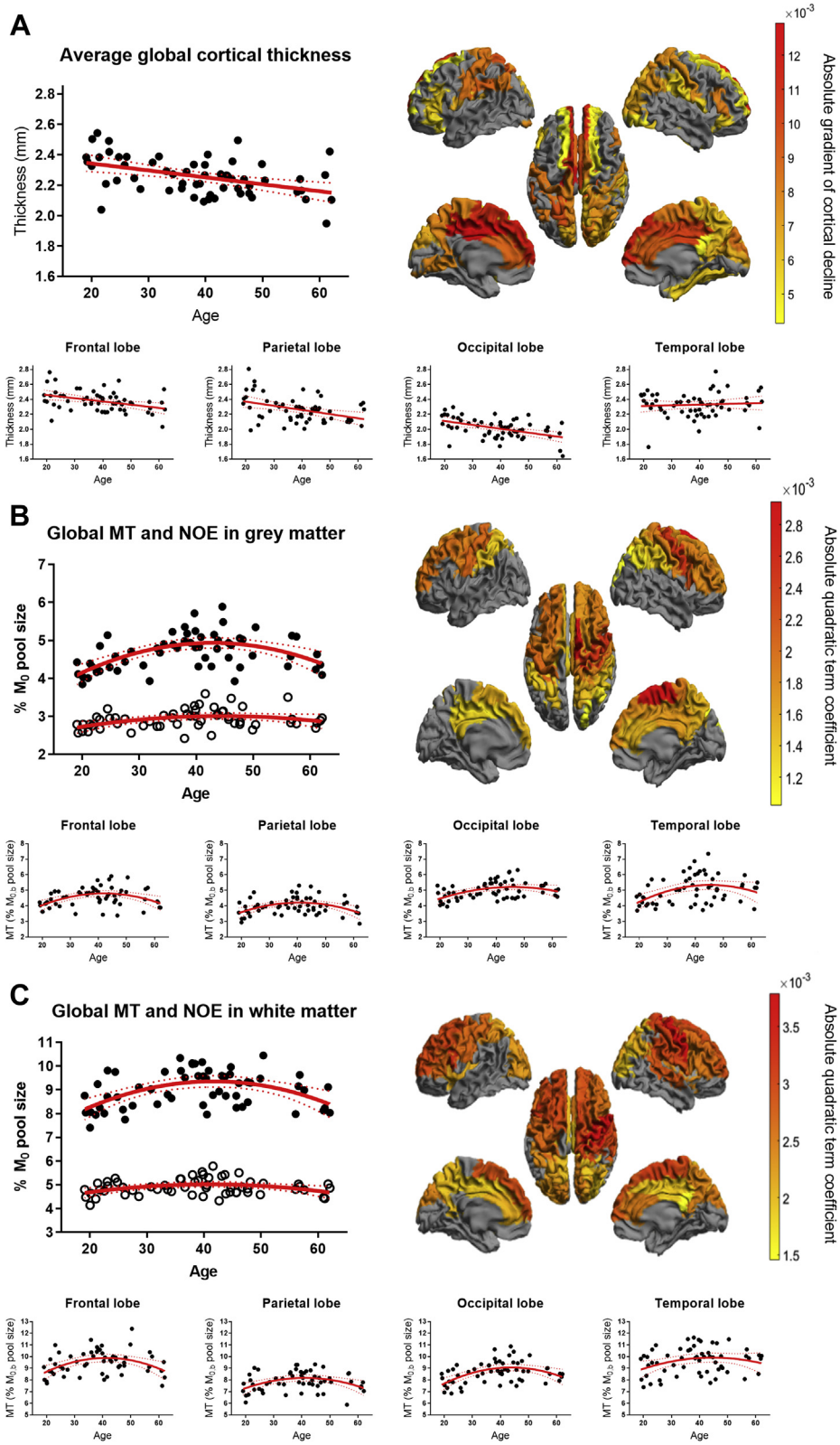

Fig. 1. Age-related differences in (A) global and lobe-wise cortical thickness, and MT (closed circles) from (B) gray matter (C) and white matter. NOE values are also shown on the global curves (open circles). Dotted lines correspond to 95% confidence intervals. Also shown is the topology of age-related differences in MT (with the white matter map projected onto overlying gray matter); regions shown in gray did not exhibit a significant quadratic or linear trend.

Table 1
Coefficients and significance of linear differences in cortical thickness with age globally across the brain and in each lobe of the brain separately

Measure	Linear coefficient (μm/y) ± 95% confidence intervals	*p*-value of linear trend
Cortical thickness		
Global	−4.6 ± 1.2	0.0004[a]
Frontal	−4.3 ± 1.4	0.0028[a]
Parietal	−5.6 ± 1.7	0.0019[a]
Occipital	−5.2 ± 1.3	0.0002[a]
Temporal	1.0 ± 1.8	0.59
Standard deviation in cortical thickness across the ROI		
Global	−0.09 ± 0.01	0.47
Frontal	−0.3 ± 0.1	0.058
Parietal	−0.1 ± 0.2	0.62
Occipital	+0.49 ± 0.19	0.015[a]
Temporal	−0.47± 0.18	0.011[a]

[a] Indicates a significant trend $p < 0.05$.

each GM region was plotted against the participant-averaged MT in the WM for the corresponding AAL-based region. This analysis was then repeated for the NOE data and the variation of T_1 with age was also investigated.

MT values for each GM-only and WM-only AAL ROI were averaged across all participants (removing age as a variable), and this was repeated for NOE, cortical thickness and T_1. To investigate the relationship between WM and GM, the GM values were plotted against the WM values for MT and NOE separately, and a linear fit was performed. To investigate the relationship between MT and NOE, MT values were linearly fitted against NOE values for all GM and WM regions together, and for GM and WM regions separately. T_1 values were also plotted against MT values in every GM region. To investigate whether cortex thickness was related to MT, a linear fit was performed to a plot of cortical thickness against GM MT.

To explore variations across the cortex, the standard deviation in the values of MT was calculated between the voxels within each ROI, and across the whole of the GM and WM was calculated for each participant. These standard deviation values were plotted against age and a quadratic fit was performed and compared to a linear regression with the F-test.

3. Results

3.1. Age-related differences in cortical thickness, MT, NOE and T1

Fig. 1A and Table 1 shows that cortical thickness reduces with age at a rate of 4.5 ± 1.2 μm per year when averaged over the whole brain ($p < 0.001$), with significant linear trends displayed in all lobes of the brain ($p < 0.002$) except the temporal lobes ($p = 0.6$), using an $\alpha = 0.05$ cutoff for determining significance.

Fig. 1B–C shows age-related differences in MT. For gray matter, a quadratic model fitted age-related trends better than a linear model for the whole brain and each of the 4 lobes (Table 2). The quadratic model also fitted better for most white matter, with the exception of the temporal lobes ($p = 0.055$). The quadratic coefficients, *p*-values and the F-test results of each of these quadratic fits across the different lobes are presented in Table 2. Fig. 1A and B show that GM MT showed a markedly different topological pattern of age-related differences in MT compared to cortical thickness.

Fig. 1B–C and Table 2 also shows that age-related trends for NOE were similar but significantly weaker than for MT. As several of the regional models were non-significant, only the global NOE trends

Table 2
Coefficients and significance of the quadratic model applied to differences in measured MT, NOE and T_1 with age globally across the brain and in each lobe of the brain separately

	Quadratic coefficient ($\times 10^{-4}$ [MT%/NOE%/T_1]^2/y) ± 95% confidence intervals	Age of peak (y)	*p*-value of quadratic trend vs. null hypothesis	*p*-value from F-test on quadratic model compared to linear model
MT				
Gray matter				
Global	−14 ± 3	42.9	0.00002[a]	0.000005[a]
Frontal	−16 ± 4	41.9	0.0008[a]	0.0005[a]
Parietal	−14 ± 4	40.6	0.0009[a]	0.0007[a]
Occipital	−11 ± 4	45.8	0.0074[a]	0.0023[a]
Temporal	−17 ± 7	45.2	0.0115[a]	0.0044[a]
White matter				
Global	−23 ± 5	41.7	0.0001[a]	0.000001[a]
Frontal	−26 ± 8	41.3	0.0011[a]	0.0008[a]
Parietal	−20 ± 6	41.1	0.0025[a]	0.0019[a]
Occipital	−24 ± 7	43.8	0.0005[a]	0.0002[a]
Temporal	−15 ± 9	44.6	0.0847	0.0546
NOE				
Gray matter				
Global	−5 ± 4	44.4	0.016[a]	0.0078[a]
Frontal	−6 ± 8	47.0	0.125	0.0711
Parietal	−6 ± 4	40.6	0.003[a]	0.0022[a]
Occipital	−3 ± 82	45.4	0.189	0.1352
Temporal	−5 ± 36	44.0	0.092	0.0641
White matter				
Global	−8 ± 5	40.9	0.005[a]	0.0041[a]
Frontal	−13 ± 9	41.6	0.005[a]	0.0033[a]
Parietal	−6 ± 7	42.8	0.066	0.0495[a]
Occipital	−5 ± 7	42.8	0.1656	0.1371
Temporal	−4 ± 0.8	37.5	0.341	0.3704
T_1				
Gray matter				
Global	1.7 ± 1.4	48.5	0.005[a]	0.0006[a]
White matter				
Global	0.74 ± 0.38	44.8	0.00002[a]	0.000004[a]

[a] Indicates a significant non-zero trend $p < 0.05$.

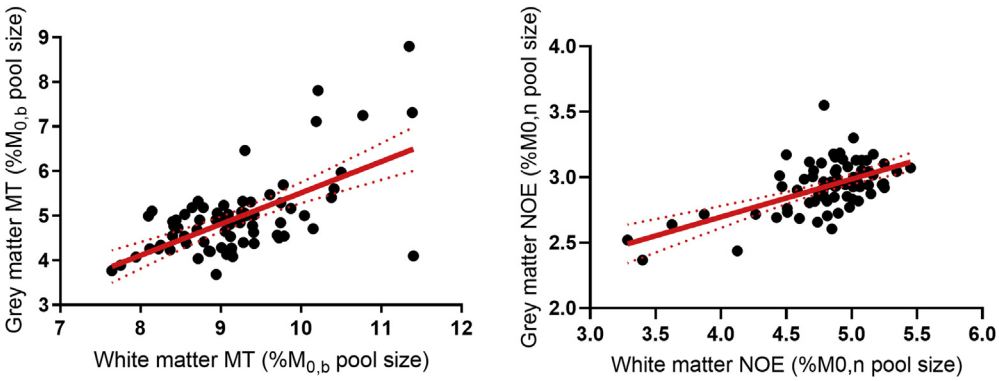

Fig. 2. Variation in MT (left) and NOE (right) in GM with that in underlying WM within the same AAL region, averaged across individuals for each AAL region.

are displayed. Fig. S1A-B and Table 2 show that T_1 also varied quadratically with age in GM and WM.

3.2. Relationship between GM and WM within same AAL region

Fig. 2 shows that the MT in each AAL ROI, averaged across participants, varied linearly with MT in the underlying WM for the same AAL region ($R^2 = 0.384$, $p < 0.0001$). A similar relationship was observed for NOE ($R^2 = 0.343$, $p < 0.0001$).

3.3. Relationship between NOE, cortical thickness, T1, and MT

Fig. S1C and D shows that in GM ROIs (averaged across participants) there was no correlation between T_1 and MT ($p > 0.9$), but a negative linear correlation was observed for WM ($p < 0.001$, $R^2 = 0.23$). If only participants aged under 42 were considered for GM then a non significant linear trend was observed ($p = 0.24$)

Fig. S2A shows that there is a strong linear relationship between MT and NOE averaging across all participants for both GM and WM ROIs ($R^2 = 0.9478$, $p < 0.0001$). This relationship was persisted when considering either GM ($R^2 = 0.305$, $p < 0.0001$) or WM ($R^2 = 0.282$, $p < 0.0001$) ROIs alone.

No significant correlation was found between cortical thickness and GM MT averaging across all participants for each ROI ($R^2 = 0.004$ and $p = 0.59$ for a linear regression). However Fig. S2B shows that when this analysis was restricted to participants under the age of 42 year old, there was a trend for cortical thickness to decrease as MT increased ($R^2 = 0.056$, $p = 0.055$).

3.4. Variation across the cortex

Fig. 3 and Tables 1 and 3 shows the variation with age in standard deviation in cortical thickness and MT values across the different regions. For cortical thickness (Fig. 3A) only the occipital and temporal lobes showed a significantly non-zero linear trend. Fig. 3B shows that the standard deviation of MT within the GM showed a significantly quadratic trend with age across the whole brain and across all lobes except for the occipital lobes. Fig. 3C shows that there was no difference in the standard deviation of MT with age in WM ($p > 0.05$; Table 3).

4. Discussion

It is well known that brain structural measures such as cortical thickness and gyrification vary with age. Here we replicate previous reports of a decrease in cortical thickness with age (Fjell et al., 2009; Hogstrom et al., 2013; Madan and Kensinger, 2016, 2018; Salat et al., 2004), and complement this with 2 additional quantitative MRI measures related to tissue composition, magnetisation transfer (MT) and Nuclear Overhauser Enhancement (NOE). MT is widely used to study demyelination in Multiple Sclerosis patients (Levesque et al., 2010), and has been proven to be strongly correlated with myelin content in the brain (Schmierer et al., 2007). Simple measures of MT such as MTR can also be affected by the T_1 of the tissue but the quantitative MT measures used here are corrected for the variations in water T_1 and hence are more specifically sensitive to myelination. This is important since T_1 decreases as either myelin or iron content increase. It is known from histology and susceptibility weighted MRI that iron deposition can continue until the age of 40 or even 60 years of age (Hallgren and Sourander, 1958; Wang et al., 2012), and increases further in older age in some deep gray matter areas (Hallgren and Sourander, 1958). In earlier life iron is required in myelin production in oligodendrocytes, but later in life the iron accumulation may be more pathological (Connor and Menzies, 1996; Todorich et al., 2009).

Our quantitative measures showed widespread differences in MT through midlife in the cortical gray and white matter, and in contrast to the linear decrease in cortical thickness, these followed a parabolic profile peaking at about 42 years of age (varying between 35-48 across different brain regions). Where as MT values are expected to increase with myelination, T_1 is expected to decrease with myelination (and with increasing iron). T_1 showed a minimum at 49 years in GM, and at 45 years in WM. The trends were similar across the whole brain but were stronger in the WM regions, possibly because of the greater absolute MT value in those regions. These results suggest that myelination increases until the age of about 40, which is consistent with evidence that the production of oligodendrocytes can be associated with learning new skills (McKenzie et al., 2014). In later life evidence from electron microscope preparations in non-human primates has related decreases in myelination to the breakdowns in the myelin sheath and white-matter integrity (Peters, 2002; Peters et al., 1996). This decrease in myelination appears to a key facet of the general cortical atrophy known to occur with aging, as other mechanisms (e.g., a reduction of cortical neurons) have been ruled out (Gefen et al., 2015; von Bartheld, 2018).

The age at which we observed peak MT agrees with the work of Yeatman et al. (Yeatman et al., 2014), who found the maximum in $1/T_1$ in WM at ~40 years. Cho et al. (1997) also found a minimum in T_1 at about 40 years in WM, but found a mimium at 60 years in cortex. We found that in general MT and NOE peaked slightly later in GM than WM but the differences were small (Table 2). However similar to Cho et al., we did observe T1 in GM to have a minimum at a later age (48.5 years). These differences between MT and T1 will reflect the opposing effects of decreasing myelination (decreases MT and increases T_1) and increasing iron (decreases T_1) in the brain in later

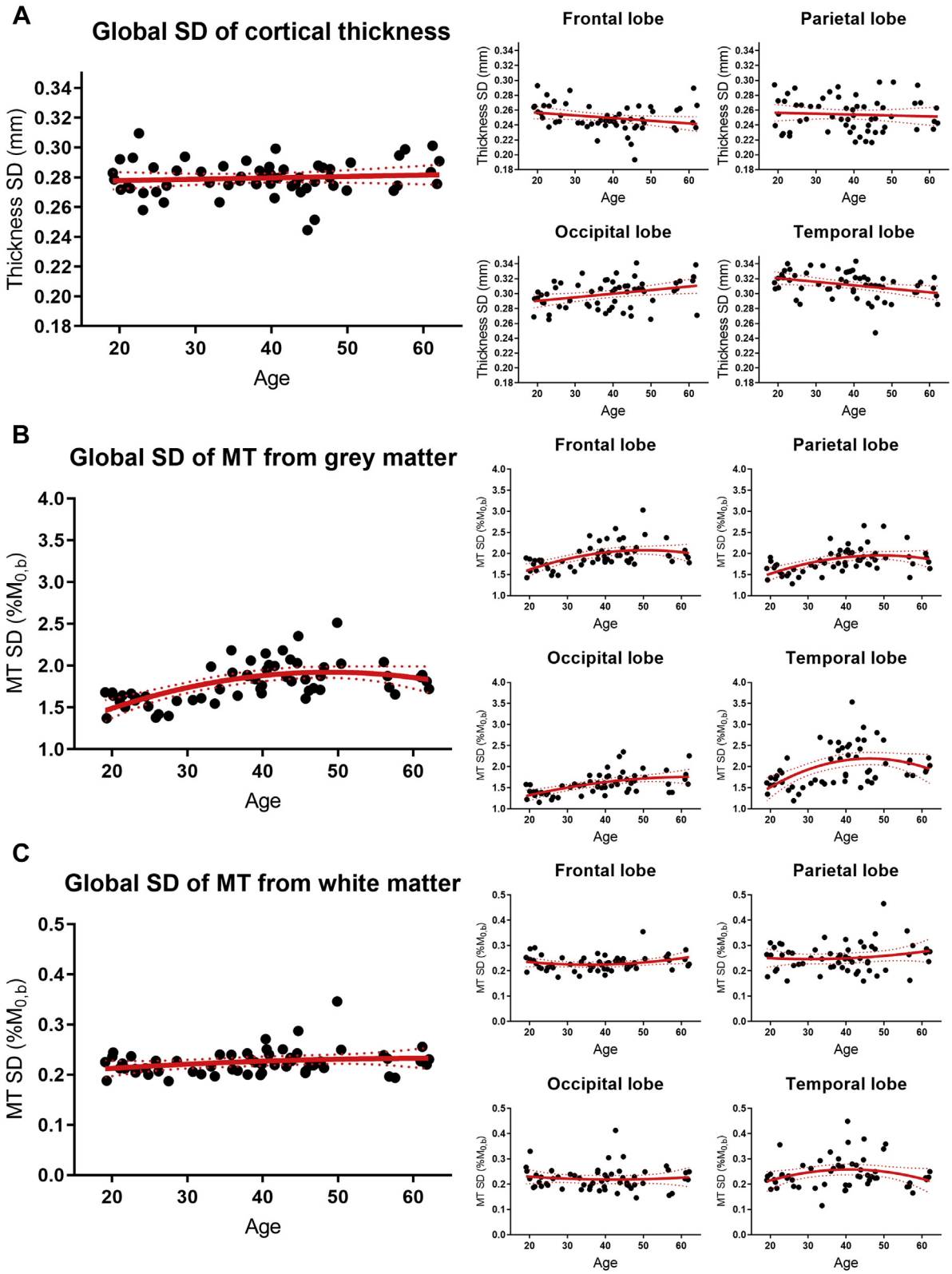

Fig. 3. Age-related variations in SD of global and lobe-wise (A) cortical thickness and MT from (B) gray matter and (C) white matter.

Table 3
Coefficients and significance of the quadratic model applied to differences in the standard deviation of measured MT with age globally across the brain and in each lobe of the brain separately

	Quadratic coefficient ($\times 10^{-4}$ MT%^{2}/y) ± 95% confidence intervals	Age of peak (y)	*p*-value of quadratic trend vs. null hypothesis	*p*-value from F-test on quadratic model compared to linear model
MT				
Gray Matter				
Global	−5 ± 1	48.90	0.000002[a]	0.000005[a]
Frontal	−5 ± 2	50.31	0.00009[a]	0.0050[a]
Parietal	−5 ± 2	49.07	0.00020[a]	0.0038[a]
Occipital	−2 ± 2	62.67	0.00004[a]	0.1756
Temporal	−9 ± 3	46.20	0.00048[a]	0.0006[a]
White matter				
Global	−0.1 ± 0.4	62.35	0.1588	0.7530
Frontal	−0.4 ± 0.2	35.54	0.1527	0.0633
Parietal	−0.3 ± 0.5	30.29	0.4868	0.6094
Occipital	−0.2 ± 0.4	42.14	0.8008	0.6879
Temporal	−0.9 ± 0.5	40.83	0.1183	0.0196[a]

[a] Indicates a significant non-zero trend $p < 0.05$.

life. The opposing effect of myelination on MT and T_1 was seen in WM (Fig. S1D) but not in GM (Fig. S1C and E) again probably reflecting the effect of varying iron concentration in GM with age and also across the cortex (Cox and Gowland, 2010), as the data is plotted for each ROI averaged across all participants. These results all suggest that quantitative MT is a more specific marker of myelination than T_1. It should be noted that some MT measures (in particular the MT Ratio) can be dependent upon T_1, but the quantitative method used here corrects for these effects (Geades et al., 2016). Furthermore, previous studies (Tyler and Gowland, 2005) have shown that the macromolecular T1 has little effect on the measured MT. The use of multiple MRI modalities (including qMT, T_1, susceptibility and T_2 mapping) (Warntjes et al., 2016) would make it easier to tease apart the differences in iron and myelination occuring in the brain with age. These findings build on previous work, such as Taubert et al. (2020), where global changes in MT have been demonstrated in both gray and white matter in relation to age, though this study examined mid-to old-age adults (ages 46-86).

We found that the value of MT in each ROI (averaged across all participants) was correlated with the MT measured in the underlying WM in the same ROI, and a similar result was found for NOE (Fig. 2). This is expected since the connectivity bewteen areas of GM is achieved primarility by axons in the underlying WM (for instance the u-fibres) and may suggest an additional means of studying connectivity.

NOE is a relatively new measure, which has also been shown to vary with myelin concentration in vivo, for example in the visual cortex (Mougin et al., 2013). The NOE signal in the brain is thought to originate in transfer of magnetisation from aliphatic backbones of mobile macromolecules and proteins, with the signal possibly relayed via molecular exchange (van Zijl et al., 2018). Here we found that MT and NOE were well correlated across all GM and WM regions suggesting that similar mechanisms were affecting them both. The fitting method used here models MT and NOE simultaneously and thus minimises biasing of the NOE signal by MT. Furthermore this fitting method has found this relationship between NOE and MT breaks down in blood where the NOE effect is relatively larger (Shah et al., 2018). This suggests that NOE is correlated to myelination independent of MT, and might relate to the fact that NOE is thought to be sensitive to the aliphatic groups in myelin. The sensitivity of the NOE signal is lower than MT, but nonetheless, this measure has not yet been explored fully and thus these results may play a role in planning future experiments.

The standard deviation in GM was an order of magnitude larger than that in white matter and it seems likely that this reflects real variation across the ROI. The GM ROIs were smaller than the WM ROIs which will have caused a larger standard error in both the mean and the standard deviation, but will not influence the participant-averaged value of standard deviation. Furthermore the absolute value of MT in GM was about half that in WM but we do not expect this to explain the increase the absolute variance in the measurement and have shown that the interindividual variability is the same in GM and WM MT measured with this method (Geades et al., 2016). There was a linear increase in standard deviation in MT values across GM with age of about 30% (dominated by the period up to the age 40), but no singificant difference in the standard deviation of MT in WM. We propose that this increase in variation in MT with age reflects ongoing cortical plasticity over this period, for instance relating to longitudinal changes in structural networks (Wu et al., 2013).

Although these results indicate that quantitative MT can be a more specific measure of myelination, caution must be excercised when measuring MT. We acquired a full z-spectrum which is a more specific measure than the conventional MT ratio (Geades et al., 2016), although the sampling frequencies chosen were optimized to measure amide proton transfer as well as NOE and MT and so more precise or quicker results could be achieved with further optimization of the sampling to study myelination in future. It is likely that MT is also dependent on other macromolecules present in tissue, for instance the MT signal will reduce with edema in pathology (Vavasour et al., 2011). A recent paper showed that the MT ratio measure (MTR) did not correlate with myelin content in an experimental model of demyelination (Fjær et al., 2015), although this experimental model used is likely to have also caused T_1 differences that will also have affected the MTR measure. Nonetheless, the MT pool size as measured here is not corrected for variations in the exchange rate of labile protons with free water, which depend on temperature and pH (Ward and Balaban, 2000), but are not expected to vary much in healthy individuals.

Finally, it is important to note that the cortical segmentation performed on a T_1-weighted scan, such that a change in T_1 could potentially shift the pial surface (for instance an increase in cortical iron with age, or myelination during development (Natu et al., 2019) could both reduce cortical thickness). Since myelination varies across the cortical layer, such a shift of the boundary of the cortical layer could bias the measurements of MT (Lorio et al., 2016), and indeed averaging across participants, ROIs with higher MT tended to be thinner which may reflect differential myelination across the cortical layer (Fig. S2B). However to limit any effect of this, we used PSIR for segmentation which has reduced sensitivity to proton density and T2* compared to the MPRAGE scan and the

voxels at the boundary of the cortical ribbon were excluded from the analysis. Future work could use a voxel based analysis to study this gray/white boundary. However no correlation could be seen between the coefficients of cortical thickness difference with age compared to MT differences with age when considering solely thin, medium or thick cortical ribbon regions, suggesting that the cortical ribbon thickness did not influence the MT results presented here.

5. Conclusion

We have used MT as a marker for myelination due to its reduced sensitivity to aspects of brain structure other than myelin, and have shown that it has a strong parabolic trend with age in both GM and WM, peaking on average at age 42. We also introduce the NOE effect as a possible marker for myelination, however further work into the true origin of this signal is necessary to explore where this measure may best be an asset.

Disclosure statement

No conflicts of interest exist.

CRediT authorship contribution statement

Andrew J. Carradus: Methodology, Software, Formal analysis, Writing - original draft, Writing - review & editing, Visualization. **Olivier Mougin:** Methodology, Formal analysis, Investigation, Writing - original draft, Writing - review & editing. **Benjamin A.E. Hunt:** Methodology, Investigation, Writing - review & editing. **Prejaas K. Tewarie:** Methodology, Investigation, Writing - review & editing. **Nicolas Geades:** Methodology, Software, Visualization. **Peter G. Morris:** Methodology, Writing - review & editing, Funding acquisition. **Matthew J. Brookes:** Conceptualization, Methodology, Investigation, Writing - review & editing, Funding acquisition. **Penny A. Gowland:** Conceptualization, Methodology, Writing - original draft, Writing - review & editing. **Christopher R. Madan:** Conceptualization, Methodology, Formal analysis, Writing - original draft, Writing - review & editing.

Acknowledgements

Andrew Carradus holds a studentship with the Haydn Green Foundation. Data collection was funded by Medical Research Council (MRC) New Investigator Research Grant MR/M006301/1, MRC Partnership Grant MR/K005464/1, and MRC Doctoral Training Grant MR/K501086/1.

Appendix A. Supplementary data

Supplementary data associated with this article can be found, in the online version, at https://doi.org/10.1016/j.neurobiolaging.2020.08.009.

References

Armstrong, T.S., Cohen, M.Z., Weinberg, J., Gilbert, M.R., 2004. Imaging techniques in neuro-oncology. Semin. Oncol. Nurs. 20, 231–239.
Bartzokis, G., Lu, P.H., Heydari, P., Couvrette, A., Lee, G.J., Kalashyan, G., Freeman, F., Grinstead, J.W., Villablanca, P., Finn, J.P., Mintz, J., Alger, J.R., Altshuler, L.L., 2012. Multimodal magnetic resonance imaging assessment of white matter aging trajectories over the lifespan of healthy individuals. Biol. Psychiatry 72, 1026–1034.
Callaghan, M.F., Freund, P., Draganski, B., Anderson, E., Cappelletti, M., Chowdhury, R., Diedrichsen, J., FitzGerald, T.H.B., Smittenaar, P., Helms, G., Lutti, A., Weiskopf, N., 2014. Widespread age-related differences in the human brain microstructure revealed by quantitative magnetic resonance imaging. Neurobiol. Aging 35, 1862–1872.
Campbell, H., 1905. Principles of heredity: a review. Br. J. Inebriety 3, 31–35.
Cho, S., Jones, D., Reddick, W.E., Ogg, R.J., Grant Steen, R., 1997. Establishing norms for age-related changes in proton T1 of human brain tissue in vivo. Magn. Reson. Imaging 15, 1133–1143.
Connor, J.R., Menzies, S.L., 1996. Relationship of iron to oligodendrocytes and myelination. Glia 17, 83–93.
Cox, E.F., Gowland, P.A., 2010. Simultaneous quantification of T_2 and T'_2 using a combined gradient echo-spin echo sequence at ultrahigh field. Magn. Reson. Med. 64, 1440–1445. https://doi.org/10.1002/mrm.22522.
Dale, A.M., Fischl, B., Sereno, M.I., 1999. Cortical surface-based analysis: I. Segmentation and surface reconstruction. Neuroimage 9, 179–194.
de Mooij, S.M.M., Henson, R.N.A., Waldorp, L.J., Kievit, R.A., 2018. Age differentiation within gray matter, white matter, and between memory and white matter in an adult life span cohort. J. Neurosci. 38, 5826–5836.
Desmond, K.L., Moosvi, F., Stanisz, G.J., 2014. Mapping of amide, amine, and aliphatic peaks in the CEST spectra of murine xenografts at 7 T. Magn. Reson. Med. 71, 1841–1853.
Dick, F., Tierney, A.T., Lutti, A., Josephs, O., Sereno, M.I., Weiskopf, N., 2012. In vivo functional and myeloarchitectonic mapping of human primary auditory areas. J. Neurosci. 32, 16095–16105.
Draganski, B., Ashburner, J., Hutton, C., Kherif, F., Frackowiak, R.S.J., Helms, G., Weiskopf, N., 2011. Regional specificity of MRI contrast parameter changes in normal ageing revealed by voxel-based quantification (VBQ). Neuroimage 55, 1423–1434.
Edzes, H.T., Samulski, E.T., 1977. Cross relaxation and spin diffusion in the proton NMR of hydrated collagen. Nature 265, 521–523.
Fischl, B., 2012. FreeSurfer. Neuroimage 62, 774–781.
Fjær, S., Bø, L., Myhr, K.M., Torkildsen, O., Wergeland, S., 2015. Magnetization transfer ratio does not correlate to myelin content in the brain in the MOG-EAE mouse model. Neurochem. Int. 83-84, 28–40.
Fjell, A.M., Walhovd, K.B., Fennema-Notestine, C., McEvoy, L.K., Hagler, D.J., Holland, D., Brewer, J.B., Dale, A.M., 2009. One-year brain atrophy evident in healthy aging. J. Neurosci. 29, 15223–15231.
Flechsig, P.E., 1920. Anatomie des menschlichen Gehirns und Rückenmarks auf myelogenetischer Grundlage, 1. G. Thieme, Leipzig.
Geades, N., Hunt, B.A.E.E., Shah, S.M., Peters, A., Mougin, O.E., Gowland, P.A., 2016. Quantitative analysis of the z-spectrum using a numerically simulated look-up table: application to the healthy human brain at 7T. Magn. Reson. Med. 78, 645–655.
Gefen, T., Gefen, T., Peterson, M., Papastefan, S.T., Martersteck, A., Whitney, K., Rademaker, A., Rademaker, A., Bigio, E.H., Bigio, E.H., Weintraub, S., Weintraub, S., Rogalski, E., Mesulam, M.M., Mesulam, M.M., Geula, C., 2015. Morphometric and histologic substrates of cingulate integrity in elders with exceptional memory capacity. J. Neurosci. 35, 1781–1791.
Glasser, M.F., Van Essen, D.C., 2011. Mapping human cortical areas *in vivo* based on myelin content as revealed by T1- and T2-weighted MRI. J. Neurosci. 31, 11597–11616.
Grydeland, H., Walhovd, K.B., Tamnes, C.K., Westlye, L.T., Fjell, A.M., 2013. Intracortical myelin links with performance variability across the human lifespan: Results from T1- and T2- weighted MRI myelin mapping and diffusion tensor imaging. J. Neurosci. 33, 18618–18630.
Hallgren, B., Sourander, P., 1958. The effect of age on the non-haemin iron in the human brain. J. Neurochem. 3, 41–51.
Hogstrom, L.J., Westlye, L.T., Walhovd, K.B., Fjell, A.M., 2013. The structure of the cerebral cortex across adult life: Age-related patterns of surface area, thickness, and gyrification. Cereb. Cortex. 23, 2521–2530.
Hopf, A., 1955. Über die Verteilung myeloarchitektonischer Merkmale in der isokortikalen Schläfenlappenrinde beim Menschen. J. Hirnforsch. 2, 36–54.
Hunt, B.A.E., Tewarie, P.K., Mougin, O.E., Geades, N., Jones, D.K., Singh, K.D., Morris, P.G., Gowland, P.A., Brookes, M.J., 2016. Relationships between cortical myeloarchitecture and electrophysiological networks. Proc. Natl. Acad. Sci. U. S. A. 113, 13510–13515.
Jones, C.K., Huang, A., Xu, J., Edden, R.A.E., Schär, M., Hua, J., Oskolkov, N., Zacà, D., Zhou, J., McMahon, M.T., Pillai, J.J., van Zijl, P.C.M., 2013. Nuclear Overhauser Enhancement (NOE) imaging in the human brain at 7 T. Neuroimage 77, 114–124.
Kaes, T., 1907. Die Grosshirnrinde des Menschen in ihren Maßen und ihrem Fasergehalt. Ein gehirnanatomischer Atlas mit erläuterndem Text. Fischer, Jena.
Levesque, I.R., Giacomini, P.S., Narayanan, S., Ribeiro, L.T., Sled, J.G., Arnold, D.L., Pike, G.B., 2010. Quantitative magnetization transfer and myelin water imaging of the evolution of acute multiple sclerosis lesions. Magn. Reson. Med. 63, 633–640.
Lorio, S., Kherif, F., Ruef, A., Melie-Garcia, L., Frackowiak, R., Ashburner, J., Helms, G., Lutti, A., Draganski, B., 2016. Neurobiological origin of spurious brain morphological changes: a quantitative MRI study. Hum. Brain Mapp. 37, 1801–1815.
Lorio, S., Lutti, A., Kherif, F., Ruef, A., Dukart, J., Chowdhury, R., Frackowiak, R.S., Ashburner, J., Helms, G., Weiskopf, N., Draganski, B., 2014. Disentangling in vivo the effects of iron content and atrophy on the ageing human brain. Neuroimage 103, 280–289.
Madan, C.R., Kensinger, E.A., 2016. Cortical complexity as a measure of age-related brain atrophy. Neuroimage 134, 617–629.
Madan, C.R., Kensinger, E.A., 2017. Age-related differences in the structural complexity of subcortical and ventricular structures. Neurobiol. Aging 50, 87–95.

Madan, C.R., Kensinger, E.A., 2018. Predicting age from cortical structure across the lifespan. Eur. J. Neurosci. 47, 399–416.

Mangeat, G., Govindarajan, S.T., Mainero, C., Cohen-Adad, J., 2015. Multivariate combination of magnetization transfer, T_2^* and B0 orientation to study the myelo-architecture of the in vivo human cortex. Neuroimage 119, 89–102. https://doi.org/10.1016/j.neuroimage.2015.06.033.

McKenzie, I.A., Ohayon, D., Li, H., De Faria, J.P., Emery, B., Tohyama, K., Richardson, W.D., 2014. Motor skill learning requires active central myelination. Science 346 (6207), 318–322.

Mougin, O., Abdel-Fahim, R., Dineen, R., Pitiot, A., Evangelou, N., Gowland, P., 2016. Imaging gray matter with concomitant null point imaging from the phase sensitive inversion recovery sequence. Magn. Reson. Med. 76, 1512–1516.

Mougin, O., Clemence, M., Peters, A., Pitiot, A., Gowland, P., 2013. High-resolution imaging of magnetisation transfer and nuclear overhauser effect in the human visual cortex at 7T. NMR Biomed. 26, 1508–1517.

Mougin, O.E., Coxon, R.C., Pitiot, A., Gowland, P.A., 2010. Magnetization transfer phenomenon in the human brain at 7 T. Neuroimage 49, 272–281.

Natu, V.S., Gomez, J., Barnett, M., Jeska, B., Kirilina, E., Jaeger, C., Zhen, Z., Cox, S., Weiner, K.S., Weiskopf, N., Grill-Spector, K., 2019. Apparent thinning of human visual cortex during childhood is associated with myelination. Proc. Natl. Acad. Sci. U. S. A. 116, 20750–20759.

Oldfield, R.C., 1971. The assessment and analysis of handedness: the Edinburgh inventory. Neuropsychologia 9, 97–113.

Peters, A., 2002. The effects of normal aging on myelin and nerve fibers: A review. J. Neurocytol. 581–593.

Peters, A., Rosene, R.L., Moss, M.B., Kemper, T.L., Abraham, C.R., Tigges, J., Albert, M.S., 1996. Neurobiological bases of age-related cognitive decline in the rhesus monkey. J. Neuropathol. Exp. Neurol. 22, 861–874.

Salat, D.H., Buckner, R.L., Snyder, A.Z., Greve, D.N., Desikan, R.S.R., Busa, E., Morris, J.C., Dale, A.M., Fischl, B., 2004. Thinning of the cerebral cortex in aging. Cereb. Cortex. 14, 721–730.

Sanchez-Panchuelo, R.M., Besle, J., Beckett, A., Bowtell, R., Schluppeck, D., Francis, S., 2012. Within-digit functional parcellation of brodmann areas of the human primary somatosensory cortex using functional magnetic resonance imaging at 7 Tesla. J. Neurosci. 32, 15815–15822.

Schmierer, K., Tozer, D.J., Scaravilli, F., Altmann, D.R., Barker, G.J., Tofts, P.S., Miller, D.H., 2007. Quantitative magnetization transfer imaging in postmortem multiple sclerosis brain. J. Magn. Reson. Imaging 26, 41–51.

Shah, S.M., Mougin, O.E., Carradus, A.J., Geades, N., Dury, R., Morley, W., Gowland, P.A., 2018. The z-spectrum from human blood at 7T. Neuroimage 167, 31–40.

Tamnes, C.K., Østby, Y., Fjell, A.M., Westlye, L.T., Due-Tønnessen, P., Walhovd, K.B., Ostby, Y., Fjell, A.M., Westlye, L.T., Due-Tønnessen, P., Walhovd, K.B., 2010. Brain maturation in adolescence and young adulthood: regional age-related changes in cortical thickness and white matter volume and microstructure. Cereb. Cortex. 20, 534–548.

Taubert, M., Roggenhofer, E., Melie-Garcia, L., Muller, S., Lehmann, N., Preisig, M., Vollenweider, P., Marques-Vidal, P., Lutti, A., Kherif, F., Draganski, B., 2020. Converging patterns of aging-associated brain volume loss and tissue microstructure differences. Neurobiol. Aging 88, 108–118.

Todorich, B., Pasquini, J.M., Garcia, C.I., Paez, P.M., Connor, J.R., 2009. Oligodendrocytes and myelination: The role of iron. Glia 57, 467–478.

Tyler, D.J., Gowland, P.A., 2005. Rapid quantitation of magnetization transfer using pulsed off-resonance irradiation and echo planar imaging. Magn. Reson. Med. 53, 103–109.

Tzourio-Mazoyer, N., Landeau, B., Papathanassiou, D., Crivello, F., Etard, O., Delcroix, N., Mazoyer, B., Joliot, M., 2002. Automated anatomical labeling of activations in SPM using a macroscopic anatomical parcellation of the MNI MRI single-subject brain. Neuroimage 15, 273–289.

van Zijl, P.C.M., Lam, W.W., Xu, J., Knutsson, L., Stanisz, G.J., 2018. Magnetization transfer contrast and chemical exchange saturation transfer MRI. Features and analysis of the field-dependent saturation spectrum. Neuroimage 168, 222–241.

Vavasour, I.M., Laule, C., Li, D.K.B., Traboulsee, A.L., MacKay, A.L., 2011. Is the magnetization transfer ratio a marker for myelin in multiple sclerosis? J. Magn. Reson. Imaging 33, 710–718.

Vogt, O., 1906. Über strukturelle hirnzentra. Mit besonderer berücksichtigung der strukturellen felder des cortex pallii [On the structural centers of the brain, with particular emphasis on the structural regions of the cortex]. Anat. Anz. 20, 74–114.

von Bartheld, C.S., 2018. Myths and truths about the cellular composition of the human brain: A review of influential concepts. J. Chem. Neuroanat. 93, 2–15.

Wang, D., Li, W. Bin, Wei, X.E., Li, Y.H., Dai, Y.M., 2012. An investigation of age-related iron deposition using susceptibility weighted imaging. PLoS One 7, e50706.

Ward, K.M., Balaban, R.S., 2000. Determination of pH using water protons and chemical exchange dependent saturation transfer (CEST). Magn. Reson. Med. 44, 799–802.

Warntjes, M., Engström, M., Tisell, A., Lundberg, P., 2016. Modeling the presence of myelin and edema in the brain based on multi-parametric quantitative MRI. Front. Neurol. 7, 16.

Wolff, S.D., Balaban, R.S., 1989. Magnetization transfer contrast (MTC) and tissue water proton relaxation in vivo. Magn. Reson. Med. 10, 135–144.

Woolrich, M.W., Jbabdi, S., Patenaude, B., Chappell, M., Makni, S., Behrens, T., Beckmann, C., Jenkinson, M., Smith, S.M., 2009. Bayesian analysis of neuroimaging data in FSL. Neuroimage 45, S173–S186.

Wu, K., Taki, Y., Sato, K., Qi, H., Kawashima, R., Fukuda, H., 2013. A longitudinal study of structural brain network changes with normal aging. Front. Human Neurosci. 7, 113.

Yeatman, J.D., Wandell, B.A., Mezer, A.A., 2014. Lifespan maturation and degeneration of human brain white matter. Nat. Commun. 5, 4932.

Zaretskaya, N., Fischl, B., Reuter, M., Renvall, V., Polimeni, J.R., 2018. Advantages of cortical surface reconstruction using submillimeter 7 T MEMPRAGE. Neuroimage 165, 11–26.